

Lepton flavour violation in constrained MSSM-seesaw models

E. Arganda, M.J. Herrero

Departamento de Física Teórica C-XI and Instituto de Física Teórica C-XVI, Universidad Autónoma de Madrid, Cantoblanco, E-28049 Madrid, Spain

We calculate the predictions for lepton flavour violating (LFV) tau and muon decays, $l_j \rightarrow l_i \gamma$, $l_j \rightarrow 3l_i$, $\mu - e$ conversion in nuclei and LFV semileptonic tau decays $\tau \rightarrow \mu PP$ with $PP = \pi^+ \pi^-, \pi^0 \pi^0, K^+ K^-, K^0 \bar{K}^0$ $\tau \rightarrow \mu P$ with $P = \pi^0, \eta, \eta'$ and $\tau \rightarrow \mu V$ with $V = \rho^0, \phi$, performing the hadronisation of quark bilinears within the chiral framework. We work within a SUSY-seesaw context where the particle content of the Minimal Supersymmetric Standard Model is extended by three right-handed neutrinos plus their corresponding SUSY partners, and where a seesaw mechanism for neutrino mass generation is implemented. Two different scenarios with either universal or non-universal soft supersymmetry breaking Higgs masses at the gauge coupling unification scale are considered. After comparing the predictions with present experimental bounds and future sensitivities, the most promising processes are particularly emphasised.

1 LFV within SUSY-seesaw models

The current knowlegde of neutrino mass differences and mixing angles clearly indicates that lepton flavour number is not a conserved quantum number in Nature. However, the lepton flavour violation (LFV) has so far been observed only in the neutrino sector. One challenging task for the present and future experiments will then be to test if there is or there is not LFV in the charged lepton sector as well.

Here we focus in the Minimal Supersymmetric Standard Model (MSSM) enlarged by three right-handed neutrinos and their SUSY partners where potentially observable LFV effects in the charged lepton sector are expected to occur. We further assume a seesaw mechanism for neutrino mass generation and use, in particular, the parameterisation proposed in ¹ where the solution to the seesaw equation is written as $m_D = Y_\nu v_2 = \sqrt{m_N^{\text{diag}}} R \sqrt{m_\nu^{\text{diag}}} U_{\text{MNS}}^\dagger$. Here, R is defined by θ_i ($i = 1, 2, 3$); $v_{1(2)} = v \cos(\sin)\beta$, $v = 174$ GeV; $m_\nu^{\text{diag}} = \text{diag}(m_{\nu_1}, m_{\nu_2}, m_{\nu_3})$ denotes the three light neutrino masses, and $m_N^{\text{diag}} = \text{diag}(m_{N_1}, m_{N_2}, m_{N_3})$ the three heavy ones. U_{MNS} is given by the three (light) neutrino mixing angles θ_{12}, θ_{23} and θ_{13} , and three phases, δ, ϕ_1 and ϕ_2 . With this parameterisation is easy to accommodate the neutrino data, while leaving room for extra neutrino mixings (from the right-handed sector). It further allows for large Yukawa couplings $Y_\nu \sim \mathcal{O}(1)$ by choosing large entries in m_N^{diag} and/or θ_i .

The predictions in the following are for two different constrained MSSM-seesaw scenarios, with universal and non-universal Higgs soft masses and with respective parameters (in addition to the previous neutrino sector parameters): 1) CMSSM-seesaw: $M_0, M_{1/2}, A_0 \tan \beta$, and $\text{sign}(\mu)$, and 2) NUHM-seesaw: $M_0, M_{1/2}, A_0 \tan \beta$, $\text{sign}(\mu)$, $M_{H_1} = M_0(1 + \delta_1)^{1/2}$ and $M_{H_2} = M_0(1 + \delta_2)^{1/2}$. All the predictions presented here include the full set of SUSY one-loop contributing diagrams and we do not use the Leading Logarithmic (LLog) nor the mass insertion approximations. The hadronisation of quark bilinears is performed within the chiral framework, using χ PT and R χ T. This is a very short summary of several publications^{2,3,4,5} to which we refer the reader for more details.

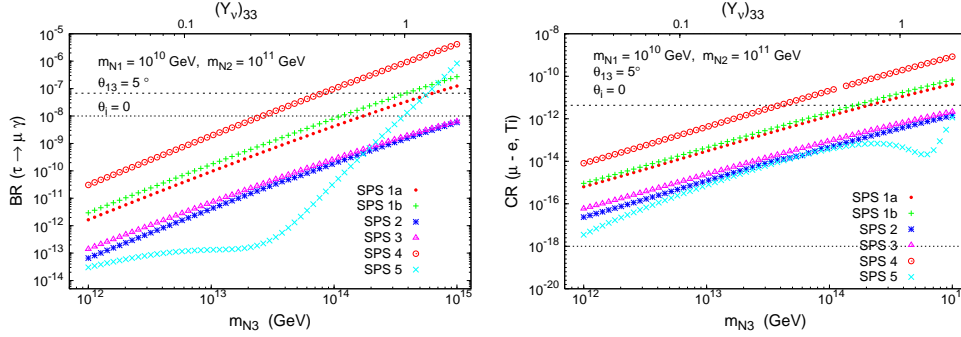


Figure 1: $\tau \rightarrow \mu\gamma$ and $\text{CR}(\mu - e, \text{Ti})$ as a function of m_{N_3} . The predictions for SPS 1a (dots), 1b (crosses), 2 (asterisks), 3 (triangles), 4 (circles) and 5 (times) are included. On the upper horizontal axis we display the associated value of $(Y_\nu)_{33}$. In each case, we set $\theta_{13} = 5^\circ$, and $\theta_i = 0$. The upper (lower) horizontal line denotes the present experimental bound (future sensitivity).

2 Results and Discussion

We focus on the dependence on the most relevant parameters which, for the case of hierarchical (degenerate) heavy neutrinos, are: the neutrino mass m_{N_3} (m_N), $\tan\beta$, θ_1 and θ_2 . We also study the sensitivity of the BRs to θ_{13} . The other input seesaw parameters m_{N_1} , m_{N_2} and θ_3 , play a secondary role since the BRs do not strongly depend on them. The light neutrino parameters are fixed to: $m_{\nu_2}^2 = \Delta m_{\text{sol}}^2 + m_{\nu_1}^2$, $m_{\nu_3}^2 = \Delta m_{\text{atm}}^2 + m_{\nu_1}^2$, $\Delta m_{\text{sol}}^2 = 8 \times 10^{-5} \text{ eV}^2$, $\Delta m_{\text{atm}}^2 = 2.5 \times 10^{-3} \text{ eV}^2$, $m_{\nu_1} = 10^{-3} \text{ eV}$, $\theta_{12} = 30^\circ$, $\theta_{23} = 45^\circ$, $\theta_{13} \lesssim 10^\circ$ and $\delta = \phi_1 = \phi_2 = 0$.

The results for the CMSSM-seesaw scenario are collected in Figs. 1 through 5. In Fig. 1, we display the predictions of $\text{BR}(\tau \rightarrow \mu\gamma)$ and $\text{CR}(\mu - e, \text{Ti})$ as a function of the heaviest neutrino mass m_{N_3} for the various SPS points, and for the particular choice $\theta_i = 0$ ($i = 1, 2, 3$) and $\theta_{13} = 5^\circ$. We have also considered the case of degenerate heavy neutrino spectra (not shown here). In both scenarios for degenerate and hierarchical heavy neutrinos, we find a strong dependence on the the heavy neutrino masses, with the expected behaviour $|m_N \log m_N|^2$ of the LLog approximation, except for SPS 5 point, which fails by a factor of $\sim 10^4$. The rates for the various SPS points exhibit the following hierarchy, $\text{BR}_4 > \text{BR}_{1b} \gtrsim \text{BR}_{1a} > \text{BR}_3 \gtrsim \text{BR}_2 > \text{BR}_5$. This behaviour can be understood in terms of the growth of the BRs with $\tan\beta$, and from the different mass spectra associated with each point. Most of the studied processes reach their experimental limit at $m_{N_3} \in [10^{13}, 10^{15}]$ which corresponds to $Y_\nu^{33,32} \sim 0.1 - 1$. At present, the most restrictive one is $\mu \rightarrow e\gamma$ (which sets bounds for SPS 1a of $m_{N_3} < 10^{13} - 10^{14} \text{ GeV}$), although $\mu - e$ conversion will be the best one in future, with a sensitivity to $m_{N_3} > 10^{12} \text{ GeV}$.

Fig. 2 shows the behaviour of the six considered LFV τ and μ decays, for SPS 4 point, as a function of $|\theta_1|$, for various values of $\arg\theta_1$. We see clearly that the BRs for $0 < |\theta_1| < \pi$ and $0 < \arg\theta_1 < \pi/2$ can increase up to a factor $10^2 - 10^4$ with respect to $\theta_i = 0$. Similar results have been found for θ_2 , while BRs are nearly constant with θ_3 in the case of hierarchical neutrinos. The behaviour of $\text{CR}(\mu - e, \text{Ti})$ with θ_i is very similar to that of $\text{BR}(\mu \rightarrow e\gamma)$ and $\text{BR}(\mu \rightarrow 3e)$. For instance, Fig. 3 shows the dependence of $\text{CR}(\mu - e, \text{Ti})$ with θ_2 , and illustrates that for large θ_2 , rates up to a factor $\sim 10^4$ larger than in the $\theta_i = 0$ case can be obtained.

In Fig. 4 we show the dependence of $\mu \rightarrow e\gamma$, $\mu \rightarrow 3e$ and $\mu - e$ conversion on the light neutrino mixing angle θ_{13} . These figures clearly manifest the very strong sensitivity of their rates to the θ_{13} mixing angle for hierarchical heavy neutrinos. Indeed, varying θ_{13} from 0 to 10° leads to an increase in the rates by as much as five orders of magnitude.

On the other hand, since $\mu \rightarrow e\gamma$ is very sensitive to θ_{13} , but $\text{BR}(\tau \rightarrow \mu\gamma)$ is clearly not, and since both BRs display the same approximate behaviour with m_{N_3} and $\tan\beta$, one can study the impact that a potential future measurement of θ_{13} and these two rates can have on the

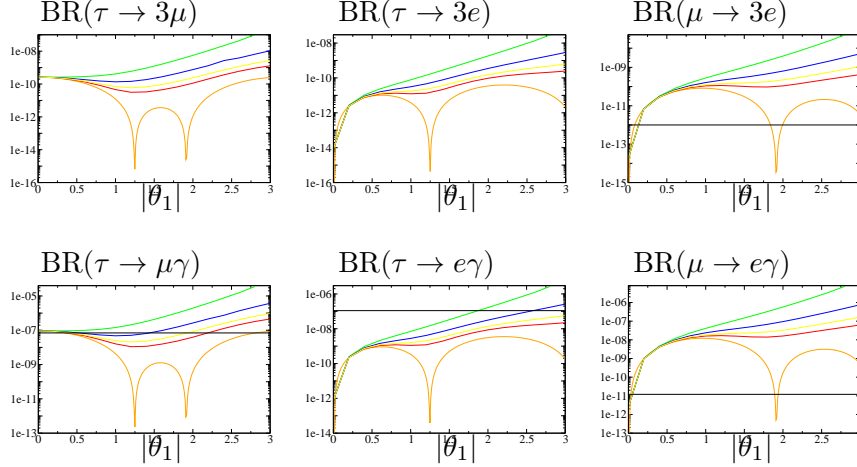


Figure 2: Dependence of LFV τ and μ decays with $|\theta_1|$ for SPS 4 case with $\arg(\theta_1) = 0, \pi/10, \pi/8, \pi/6, \pi/4$ in radians (lower to upper lines), $(m_{N_1}, m_{N_2}, m_{N_3}) = (10^8, 2 \times 10^8, 10^{14})$ GeV, $\theta_2 = \theta_3 = 0$, $\theta_{13} = 0$ and $m_{\nu_1} = 0$. The horizontal lines are the present experimental bounds.

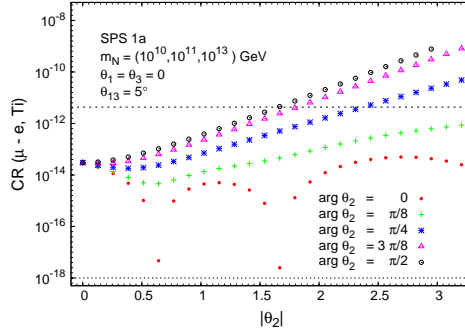


Figure 3: $CR(\mu - e, Ti)$ as a function of $|\theta_2|$, for SPS 1a case with $\arg \theta_2 = \{0, \pi/8, \pi/4, 3\pi/8, \pi/2\}$ (dots, crosses, asterisks, triangles and circles, respectively), $m_{N_i} = (10^{10}, 10^{11}, 10^{13})$ GeV, $\theta_{13} = 5^\circ$. The upper (lower) horizontal line denotes the present experimental bound (future sensitivity).

knowledge of the otherwise unreachable heavy neutrino parameters. The correlation of these two observables as a function of m_{N_3} , is shown in Fig. 5 for SPS 1a. Comparing these predictions for the shaded areas along the expected diagonal “corridor”, with the allowed experimental region, allows to conclude about the impact of a θ_{13} measurement on the allowed/excluded m_{N_3} values. The most important conclusion from Fig. 5 is that for SPS 1a, and for the parameter space defined in the caption, an hypothetical θ_{13} measurement larger than 1° , together with the present experimental bound on the $BR(\mu \rightarrow e \gamma)$, will have the impact of excluding values of $m_{N_3} \gtrsim 10^{14}$ GeV. Moreover, with the planned MEG sensitivity, the same θ_{13} measurement could further exclude $m_{N_3} \gtrsim 3 \times 10^{12}$ GeV.

The numerical results for the NUHM-seesaw scenario as a function of $M_0 = M_{1/2} = M_{\text{SUSY}}$ are collected in Figs. 6 and 7. The behaviour of the predicted m_{H^0} as a function of M_{SUSY} is shown in Fig. 6 (left panel). The most interesting solutions with important phenomenological implications are found for negative δ_1 and positive δ_2 . Notice that, for all the explored $\delta_{1,2}$ values, we find a value of m_{H^0} that is significantly smaller than in the universal case ($\delta_{1,2} = 0$).

In Fig. 6 (right panel) the various contributions from the γ -, Z -, Higgs mediated penguins and box diagrams as a function of M_{SUSY} are shown. Here, we choose $\delta_1 = -1.8$ and $\delta_2 = 0$. We observe a very distinct behaviour with M_{SUSY} of the Higgs-mediated contributions compared to those of the CMSSM case. In fact, the Higgs-mediated contribution can equal, or even exceed that of the photon, dominating the total conversion rate in the large $M_0 = M_{1/2}$ region.

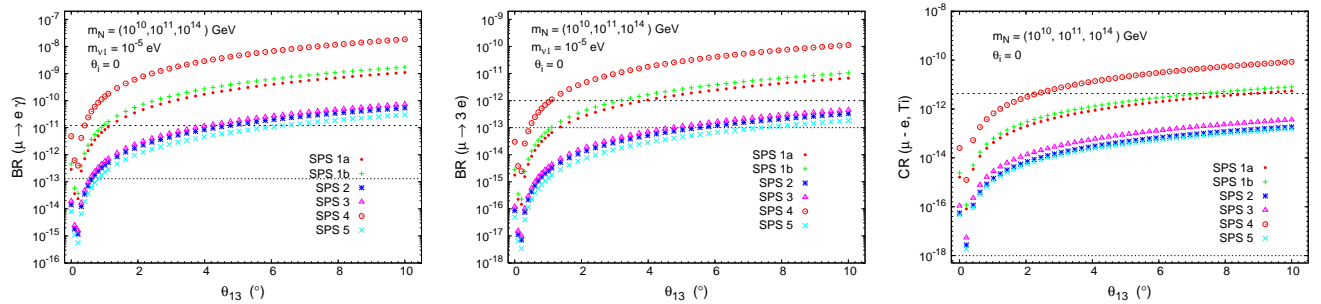


Figure 4: $\text{BR}(\mu \rightarrow e\gamma)$, $\text{BR}(\mu \rightarrow 3e)$ and $\text{CR}(\mu - e, \text{Ti})$ as a function of θ_{13} (in degrees), for SPS 1a (dots), 1b (crosses), 2 (asterisks), 3 (triangles), 4 (circles) and 5 (times), with $\theta_i = 0$ and $m_{N_i} = (10^{10}, 10^{11}, 10^{14})$ GeV. The upper (lower) horizontal line denotes the present experimental bound (future sensitivity).

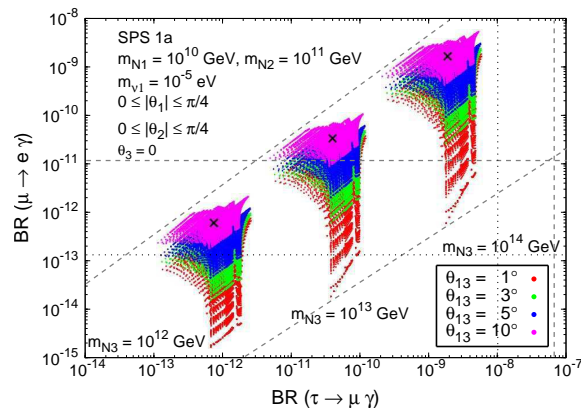


Figure 5: Correlation between $\text{BR}(\mu \rightarrow e\gamma)$ and $\text{BR}(\tau \rightarrow \mu\gamma)$ as a function of m_{N_3} , for SPS 1a, and impact of θ_{13} . The areas displayed represent the scan over θ_i . From bottom to top, the coloured regions correspond to $\theta_{13} = 1^\circ, 3^\circ, 5^\circ$ and 10° (red, green, blue and pink, respectively). Horizontal and vertical dashed (dotted) lines denote the experimental bounds (future sensitivities).

These larger Higgs contributions are the consequence of their exclusive SUSY non-decoupling behaviour for large M_{SUSY} , and of the lighter Higgs boson mass values encountered in this region, as previously illustrated in Fig. 6.

In Fig. 7 we display the predicted $\mu - e$ conversion rates for other nuclei, concretely Al, Ti, Sr, Sb, Au and Pb, as a function of M_{SUSY} . We clearly see that $\text{CR}(\mu - e, \text{Sb}) > \text{CR}(\mu - e, \text{Sr}) > \text{CR}(\mu - e, \text{Ti}) > \text{CR}(\mu - e, \text{Au}) > \text{CR}(\mu - e, \text{Pb}) > \text{CR}(\mu - e, \text{Al})$. The most important conclusion from Fig. 7 is that we have found predictions for Gold nuclei which, for the input parameters in this plot, are above its present experimental bound throughout the explored M_{SUSY} interval. Finally, although not shown here for shortness, we have also found an interesting loss of correlation between the predicted $\text{CR}(\mu - e, \text{Ti})$ and $\text{BR}(\mu \rightarrow e\gamma)$ in the NUHM-seesaw scenario compared to the universal case where these are known to be strongly correlated. This loss of correlation occurs when the Higgs-contributions dominate the photon-contributions and could be tested if the announced future sensitivities in these quantities are reached.

The corresponding predictions for $\theta_2 = 2.9e^{i\pi/4}$ of the nine LFV semileptonic τ decays studied in this work as a function of M_{SUSY} are shown in Fig. 8. In this case, we work with $\delta_1 = -2.4$ and $\delta_2 = 0.2$, that drive us to Higgs boson masses around 150 GeV even for heavy SUSY spectra. In this Fig. 8 we can see that, the choice of θ_2 increase all the rates about two orders of magnitude respect to the case $\theta_i = 0$, not shown here for brevity. $\text{BR}(\tau \rightarrow \mu\pi^+\pi^-)$ and $\text{BR}(\tau \rightarrow \mu\rho)$ get the largest rates and, indeed, the predictions of these two latter channels

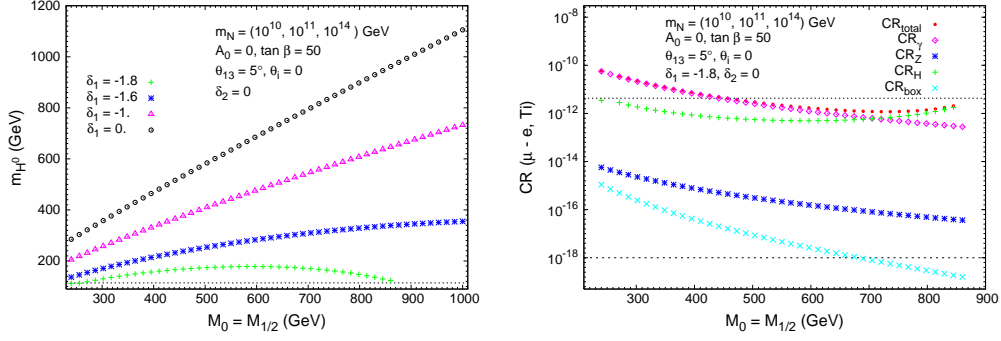


Figure 6: Left panel: Mass of m_{H^0} as a function of $M_0 = M_{1/2}$, for fixed values of $\delta_1 = \{-1.8, -1.6, -1, 0\}$ (respectively crosses, asterisks, triangles and circles), with $m_{N_i} = (10^{10}, 10^{11}, 10^{14})$ GeV, $\theta_i = 0$, $A_0 = 0$, $\tan \beta = 50$ and $\theta_{13} = 5^\circ$. Right panel: Contributions to $CR(\mu - e, Ti)$: total (dots), γ -penguins (diamonds), Z -penguins (asterisks), H -penguins (crosses) and box diagrams (times) as a function of $M_0 (= M_{1/2})$ for the NUHM case with $\delta_1 = -1.8$, $\delta_2 = 0$, $\tan \beta = 50$, $m_{N_i} = (10^{10}, 10^{11}, 10^{14})$ GeV, $\theta_{13} = 5^\circ$ and $R = 1$ ($\theta_i = 0$). The upper (lower) horizontal line denotes the present experimental bound (future sensitivity).

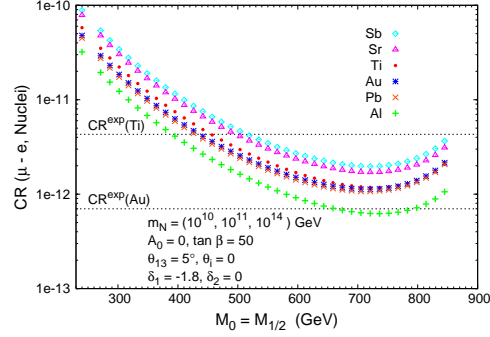


Figure 7: $\mu - e$ conversion rates as a function of $M_0 = M_{1/2}$ in the NUHM-seesaw for various nuclei: Sb, Sr, Ti, Au, Pb and Al nuclei (diamonds, triangles, dots, asterisks, times and crosses, respectively), with $m_{N_i} = (10^{10}, 10^{11}, 10^{14})$ GeV, $A_0 = 0$, $\tan \beta = 50$, $\theta_{13} = 5^\circ$, $\theta_i = 0$, $\delta_1 = -1.8$ and $\delta_2 = 0$. From top to bottom, the horizontal dashed lines denote the present experimental bounds for $CR(\mu - e, Ti)$ and $CR(\mu - e, Au)$.

reach their present experimental sensitivities at the low M_{SUSY} region, below 200 GeV and 250 GeV respectively, for this particular choice of input parameters.

In Fig. 9 we plot finally the predictions for $BR(\tau \rightarrow \mu K^+ K^-)$ and $BR(\tau \rightarrow \mu \eta)$ as a function of one of the most relevant parameters for these Higgs-mediated processes which is the corresponding Higgs boson mass.

Firstly, we see that the approximate (see the approximate formulae in ⁵) and exact results of the Higgs contribution agree within a factor of two for both channels, but the agreement of the full result with respect to the Higgs contribution is clearly worse in the case of $\tau \rightarrow \mu K^+ K^-$ than in $\tau \rightarrow \mu \eta$. In the latter, the agreement is quite good because the Z -mediated contribution is negligible, and this holds for all M_{SUSY} values in the studied interval, $250 \text{ GeV} < M_{SUSY} < 750 \text{ GeV}$. In the first, it is only for large M_{SUSY} that the H -mediated contribution competes with the γ -mediated one and the Higgs rates approach the total rates. For instance, the predictions for $BR(\tau \rightarrow \mu K^+ K^-)$ shows that for $M_{SUSY} = 750 \text{ GeV}$ and $m_{H^0} = 160 \text{ GeV}$ the total rate is about a factor 2 above the Higgs rate, but for $m_{H^0} = 240 \text{ GeV}$ it is already more than a factor 5 above.

In this figure we have also explored larger values of m_{N_3} and $\tan \beta$, by using in those cases the approximate formula, and in order to conclude about the values that predict rates comparable with the present experimental sensitivity. We can conclude then that, at present, it is certainly

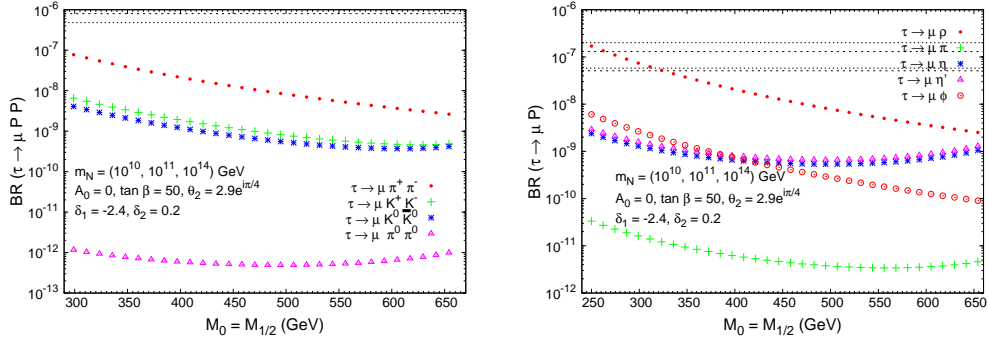


Figure 8: Predictions of $\text{BR}(\tau \rightarrow \mu PP)$ and $\text{BR}(\tau \rightarrow \mu P)$ as a function of M_{SUSY} in the NUHM scenario for a large $\tau - \mu$ mixing driven by $\theta_2 = 2.9e^{i\pi/4}$.

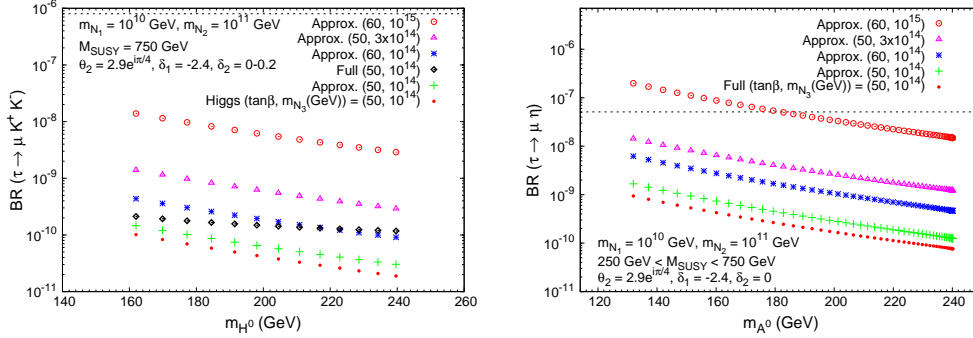


Figure 9: Predictions for $\text{BR}(\tau \rightarrow \mu K^+ K^-)$ and $\text{BR}(\tau \rightarrow \mu \eta)$ as a function of m_{H^0} in the NUHM scenario.

$\tau \rightarrow \mu \eta$ the most competitive LFV semileptonic tau decay channel. The parameter values that provide rates being comparable to the present sensitivities in this channel are $\tan \beta = 60$ and $m_{N_3} = 10^{15}$ GeV which correspond to $|\delta_{32}| \simeq 2$.

Interestingly, the most competitive channels to explore simultaneously LFV $\tau - \mu$ transitions and the Higgs sector are $\tau \rightarrow \mu \eta$, $\tau \rightarrow \mu \eta'$ and also $\tau \rightarrow \mu K^+ K^-$. Otherwise, the golden channels to tackle the Higgs sector are undoubtedly $\tau \rightarrow \mu \eta$ and $\tau \rightarrow \mu \eta'$. On the other hand, the rest of the studied semileptonic channels, $\tau \rightarrow \mu \pi^+ \pi^-$, etc., will not provide additional information on LFV with respect to that provided by $\tau \rightarrow \mu \gamma$.

In conclusion, we believe that a joint measurement of the LFV branching ratios, the $\mu - e$ conversion rates, θ_{13} and the SUSY spectrum will be a powerful tool for shedding some light on the otherwise unreachable heavy neutrino parameters. Furthermore, in the case of a NUHM scenario, it may also provide interesting information on the Higgs sector. It is clear from this study that the connection between LFV and neutrino physics will play a relevant role for the searches of new physics beyond the SM.

We acknowledge Ana M. Teixeira, Stefan Antusch and Jorge Portolés for their participation in our works. E. Arganda thanks the organizers for his invitation to this fruitful conference.

1. J. A. Casas and A. Ibarra, Nucl. Phys. B 618 (2001) 171 [arXiv:hep-ph/0103065].
2. E. Arganda and M. J. Herrero, Phys. Rev. D **73** (2006) 055003 [arXiv:hep-ph/0510405].
3. S. Antusch, E. Arganda, M. J. Herrero and A. M. Teixeira, JHEP **0611** (2006) 090 [arXiv:hep-ph/0607263].
4. E. Arganda, M. J. Herrero and A. M. Teixeira, JHEP **0710** (2007) 104 [arXiv:0707.2955 [hep-ph]].

5. E. Arganda, M. J. Herrero and J. Portoles, JHEP **0806** (2008) 079 [arXiv:0803.2039 [hep-ph]].